Nuclear Physics B178 (1981) 421–456

THE PERTURBATIVE CALCULATION OF JET STRUCTURE IN e^+e^- ANNIHILATION*

R.K. ELLIS[1], D.A. ROSS[2] and A.E. TERRANO

California Institute of Technology, Pasadena, California 91125, USA

Received 4 July 1980

We calculate the $O(\alpha_s^2)$ corrections to the event shape in e^+e^- annihilation due to the parton processes $e^+e^- \to q\bar{q}G$, $e^+e^- \to \bar{q}\bar{q}qq$ and $e^+e^- \to q\bar{q}GG$. The event shape is characterized in an invariant way in terms of eigenvalues of an infrared-finite tensor. Working in the $\overline{\text{MS}}$ renormalization prescription the correction to the number of three-jet events is large. Reliable perturbative results will require the resummation of large terms.

1. Introduction

The observation in e^+e^- annihilation of planar hadronic events [1] whose three-jet structure can be interpreted as the result of gluon bremsstrahlung from a quark-antiquark pair, directly reveals the constituent structure of the QCD field theory. The departure of the observed final hadronic state from a simple two-jet configuration is proportional to the coupling of gluons to quarks in QCD perturbation theory and therefore is a sensitive measure of the strong coupling constant α_s. In this paper we calculate the first radiative correction ($O(\alpha_s^2)$) to the three-jet structure necessary for the meaningful determination of $\alpha_s(Q^2)$ or equivalently the scale parameter of the strong interactions Λ.

Since the original proposal [2] that event shapes in e^+e^- annihilation would provide evidence for gluons, many variables [3, 4] have been suggested to describe the jet structure of the final-state hadrons. A theoretically acceptable variable must be insensitive to the emission of soft and/or collinear radiation. Variables, which combine parallel momenta linearly, are free from mass singularities and infrared divergences and hence are reliably calculable in a perturbation series [5] in $\alpha_s(Q^2)$.

The analysis we present calculates the shape of an e^+e^- hadronic event due to the production of massless quarks and gluons, instead of in terms of the observed

* Work supported in part by the US Department of Energy under contract no. DE-AC-03-79ER0068.

[1] Address after September 1980, Theory Division, CERN, Geneva, Switzerland.

[2] Address after October 1980, Physics Department, University of Southampton, Southampton, SO9 5NH, United Kingdom.

particles which are hadrons and leptons with finite mass. Thus a further requirement to impose on jet variables is that they should be insensitive to the process of hadronization. At asymptotic energies this is certainly true since the effects of hadronization fall like powers of the c.m. energy Q relative to the leading terms. At presently investigated values of Q, understanding of the non-perturbative effects associated with hadronization is crucial to the extraction of information about the strong coupling constant. The interpretation of the experimental data also requires the inclusion of corrections due to the finite angular and energy acceptances of the particle detection equipment. Moreover, the shape of the final state is influenced by the proximity of heavy quark thresholds and the decay of resonant states (e.g., ρ, $J/\psi, \Upsilon$). None of the above effects are included in our present analysis.

Nevertheless the calculation of the effects of *perturbative* QCD is a prerequisite for a complete analysis of event shapes in $e^+e^- \to$ hadrons. It is therefore this question which we address here.

We present our results in terms of global event shape parameters which do not require the determination of a jet axis. This gives a characterization of the event shape in terms of a continuous range of the parameter; no statement need be made about which jet a given hadron belongs to. Furthermore, no minimization program (which for a large event multiplicity can be very costly in computer time) is required. Our results are presented in detail to allow the reader to extend them to include the effects which we have neglected.

We consider first of all the 3×3 tensor [6, 7],

$$\theta^{ij} = \sum_a \frac{P_a^i P_a^j}{|P_a|} \Big/ \sum_a |P_a|, \tag{1.1}$$

where the sum on a runs over all final-state hadrons and P_a^i is the c.m. three-momentum of the ath hadron*. By principal axes transformation we can reduce θ to a diagonal tensor, the eigenvalues of which are given by the roots of the characteristic equation**,

$$\lambda^3 - \lambda^2 + \tfrac{1}{3}C\lambda - \tfrac{1}{27}D = 0, \tag{1.2}$$

where we have used the condition that θ is normalized to have unit trace. In terms of the eigenvalues of θ, C and D are given by

$$D = 27\lambda_1\lambda_2\lambda_3, \qquad C = 3(\lambda_1\lambda_2 + \lambda_2\lambda_3 + \lambda_3\lambda_1). \tag{1.3}$$

* This tensor differs from the tensor used by Wu and Zobernig (ref. [8]) which is not linear in collinear momenta. Their tensor is not finite in QCD perturbation theory.

** The factors of $\frac{1}{3}$ and $\frac{1}{27}$ are included so the variables span the range from 0 to 1.

For a two-jet event both C and D vanish, whilst for a planar event,

$$C = 3\lambda_1(1-\lambda_1), \tag{1.4}$$

and D vanishes. Hence the distribution in the variable C provides an effective measure of the multijet structure of the event with special emphasis on planar events. The distribution in D measures the deviation from planarity of the events. In fig. 1 we display the contours of constants C and D on the eigenvalue plot. By imposing $C > \frac{1}{2}$ we exclude the two-jet region.

An alternative way to measure the structure of events is with the shape parameters [4],

$$H_l = \frac{4\pi}{2l+1} \sum_{m=-l}^{m=l} \left| \sum_a Y_l^m(\Omega_a) \frac{|P_a|}{Q} \right|^2 . \tag{1.5}$$

In eq. (1.5) the variable a is summed over all final-state hadrons and P_a is the c.m. three-momentum of the ath hadron and Ω_a the angle between its direction of motion and an arbitrary fixed axis. The first non-trivial shape parameter is H_2

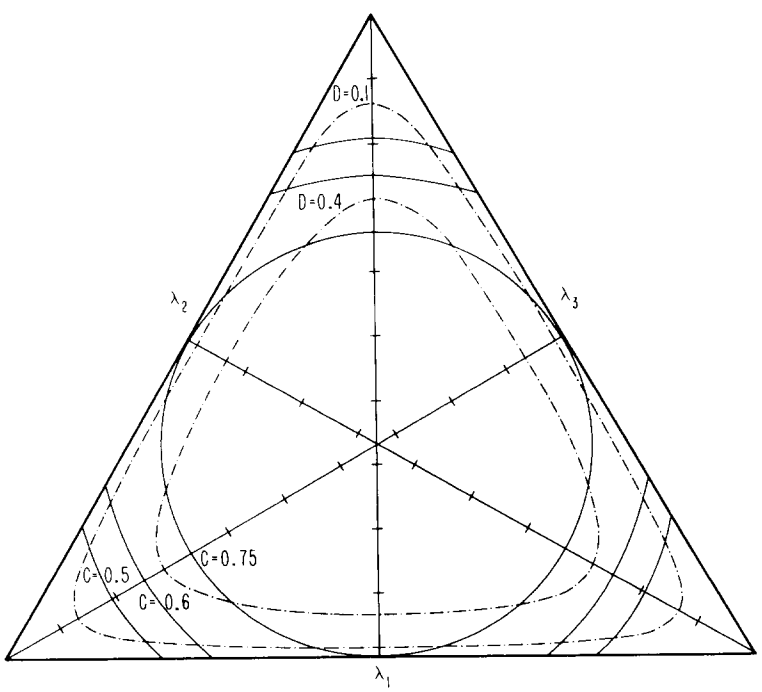

Fig. 1. Eigenvalue plot showing lines of constants C and D. By imposing $C > \frac{1}{2}$ we exclude the two-jet region. For $\lambda_1 > \lambda_2 > \lambda_3$ only the top right-hand triangle is populated.

which may also be written

$$H_2 = \sum_{a,b} \frac{|P_a||P_b|}{Q^2} P_2(\cos\theta_{ab}), \tag{1.6}$$

where P_2 is the second Legendre polynomial. Eq. (1.5) does not distinguish between events differing by the emission of soft and/or collinear particles and hence will be free of divergences in perturbation theory.

By expansion of the tensor θ^{ij} in spherical tensors we may easily show that two of the measures of event structure we have discussed are identical,

$$C \equiv (1 - H_2). \tag{1.7}$$

This identity is extremely useful. The quantity C is easier to visualize because it is related to the reduction to principal axes of a momentum ellipsoid; on the other hand, eq. (1.6) for H_2 is a more convenient starting point for perturbative calculations since it is more readily cast into covariant form.

We now turn to the evaluation of the distribution of C or $(1 - H_2)$ in the perturbation theory of quarks and gluons. We consider the reactions,

$$e^+e^- \to \gamma^*(Q) \to q\bar{q}, q\bar{q}G, q\bar{q}GG, q\bar{q}q\bar{q}, \tag{1.8}$$

and we denote the final-state parton momenta by p_i, where,

$$s_{ij} = (p_i + p_j)^2, \qquad s_{ijk} = (p_i + p_j + p_k)^2, \qquad y_{ij} = s_{ij}/Q^2, \qquad (i < j < k), \tag{1.9}$$

and since we take the masses of partons to be zero, $p_i^2 = 0$.

In analogy with eq. (1.1) we construct a tensor from the parton variables of the final state,

$$\bar{\theta}^{ij} = \sum_{\text{partons } a} \frac{p_a^i p_a^j}{|p_a|} \Big/ \sum_{\text{partons } a} |p_a|. \tag{1.10}$$

The tensor $\bar{\theta}$ which we calculate perturbatively differs only from the tensor θ by terms which vanish as an inverse power of the total c.m. energy,

$$\theta^{ij} = \bar{\theta}^{ij} + O(1/Q). \tag{1.11}$$

In complete analogy with the preceding discussion we can define the variables C and D for the tensor $\bar{\theta}$. The C parameters are given (for two-, three- and

four-particle final states, respectively) by,

$$C^{(2)} = 0, \tag{1.12}$$

$$C^{(3)} = 3\left[1 - \sum_{\substack{i,j=1 \\ i<j}}^{3} \frac{s_{ij}^2}{(2p_i\cdot Q)(2p_j\cdot Q)}\right]$$

$$= \frac{6s_{12}s_{13}s_{23}}{(s_{12}+s_{13})(s_{12}+s_{23})(s_{13}+s_{23})}, \tag{1.13}$$

$$C^{(4)} = 3\left\{1 - \sum_{\substack{i,j=1 \\ i<j}}^{4} \frac{s_{ij}^2}{(2p_i\cdot Q)(2p_j\cdot Q)}\right\}. \tag{1.14}$$

As a confirmation of our assertion that C is infrared finite, we may explicitly demonstrate that $C^{(4)}$ assumes the same form as $C^{(3)}$ in the region of collinear or soft emission by taking the appropriate limit. In the limit in which, for example, particles three and four become collinear, eq. (1.14) becomes

$$C^{(4)} \to \frac{6s_{134}s_{234}(Q^2 - s_{134} - s_{234})}{(Q^2 - s_{134})(Q^2 - s_{234})(s_{134}+s_{234})}, \qquad \begin{matrix} s_{34} = 0, \\ s_{134}, s_{234} \text{ fixed}. \end{matrix} \tag{1.15}$$

Making the identification $s_{134} = s_{13}$ and $s_{234} = s_{23}$, eq. (1.15) reduces to eq (1.13). The covariant expression for the variable D is given for a four-parton final state by

$$D^{(4)} = 27\left[\frac{2(s_{12}s_{13}s_{24}s_{34} + s_{12}s_{14}s_{23}s_{34} + s_{13}s_{14}s_{23}s_{24}) - (s_{12}^2s_{34}^2 + s_{13}^2s_{24}^2 + s_{14}^2s_{23}^2)}{(s_{12}+s_{13}+s_{14})(s_{12}+s_{23}+s_{24})(s_{13}+s_{23}+s_{34})(s_{14}+s_{24}+s_{34})}\right]. \tag{1.16}$$

The structure of this paper is as follows. In sect. 2 we calculate the differential cross section for processes involving three particles in the final state. Representing this as $\sigma^{(3)}$ we obtain the distribution in C:

$$\frac{d\sigma^{(3)}}{dC} = \int d\sigma^{(3)}\,\delta(C - C^{(3)}), \tag{1.17}$$

where $C^{(3)}$ is the expression given by eq. (1.13). The above expression contains divergences due to the emission of soft and collinear particles. In sect. 3 we calculate the contribution to the cross section due to the production of four partons

in the final state. This may be schematically written as

$$\frac{d\sigma^{(4)}}{dC} = \int d\sigma^{(4)} \delta(C - C^{(4)}), \tag{1.18}$$

where $C^{(4)}$ is given by eq. (1.14). Eq. (1.8) also contains singularities in the three-jet region. Thus the total contribution is given by,

$$\frac{d\sigma}{dC} = \frac{d\sigma^{(4)}}{dC} + \frac{d\sigma^{(3)}}{dC} \qquad C \neq 0$$

$$= d\sigma^{(4)} \delta(C - C^{(4)}) + d\sigma^{(3)} \delta(C - C^{(3)}). \tag{1.19}$$

As a calculational device it is convenient to deal only with finite quantities. Hence we evaluate the terms in $d\sigma^{(4)}$ which contain singularities in the region in which four jets masquerade as three:

$$d\sigma^{(4)} \overset{\text{singular region}}{\rightarrow} d\sigma^{(s)}. \tag{1.20}$$

We thus rewrite eq. (1.19):

$$\frac{d\sigma}{dC} = \left[d\sigma^{(4)} \delta(C - C^{(4)}) - d\sigma^{(s)} \delta(C - C^{(3)}) \right] + \left[(d\sigma^{(s)} + d\sigma^{(3)}) \delta(C - C^{(3)}) \right]. \tag{1.21}$$

Each of the terms in square brackets is now finite in the three-jet region [but still contains divergences in the two-jet region ($C = 0$)]; the first is finite by construction and the second by virtue of KLN theorem [9]. The calculation of $d\sigma/dD$ is much less complex because for $D \neq 0$ it receives contributions from $d\sigma^{(4)}$ alone. In sect. 4 we present our numerical results for the above distributions. Our conclusions are presented in sect. 5.

2. Processes involving two and three particles in the final state

As explained in sect. 1 our operating procedure is to calculate the contributions to the event shape of the various processes*:

$$e^+e^- \rightarrow q(p_1) + \bar{q}(p_2), \tag{2.1}$$

$$e^+e^- \rightarrow q(p_1) + \bar{q}(p_2) + G(p_3), \tag{2.2}$$

$$e^+e^- \rightarrow q(p_1) + \bar{q}(p_2) + G(p_3) + G(p_4), \tag{2.3}$$

$$e^+e^- \rightarrow \bar{q}(p_1) + \bar{q}(p_2) + q(p_3) + q(p_4), \tag{2.4}$$

* The four-jet reactions, eqs. (2.3), (2.4) have also been considered in ref. [10] and DeGrand, Ng and Tye [3].

where the symbols in brackets denote the momenta which we assign to the various particles. In this section we present our results for eq. (2.2). Our treatment of the processes with four particles in the final state is given in sect. 3.

There exists a certain region of phase space, corresponding to the soft or collinear emission of a gluon in which the three-jet process shown in figs. 2b, c, simulates a two-jet event shown in fig. 2a. This is precisely the region in which the intermediary propagators vanish and individual transition probabilities contain divergences, which vanish in the total transition probability after the inclusion of virtual gluon exchange as a consequence of the KLN theorem [9]. We choose to regulate these divergences, as well as the normal ultraviolet divergences by continuing the dimensionality [11] of spacetime n to $n = (4 - 2\varepsilon)$. In this scheme the phase space for the massless final-state particles is modified so that

$$(\mathrm{PS})^{(j)} = (2\pi)^n \int \left[\prod_{i=1}^{j} \frac{\mathrm{d}^n p_i}{(2\pi)^{n-1}} \delta^+(p_i^2) \right] \delta^n\left(Q - \sum_{i=1}^{j} p_i \right). \tag{2.5}$$

After performing angular integrations we obtain

$$(\mathrm{PS})^{(2)} = A_0 \int \mathrm{d}s_{12}\, \delta(y_{12} - 1) \frac{1}{4Q^4}, \tag{2.6}$$

$$(\mathrm{PS})^{(3)} = \frac{A_0}{8} \left(\frac{1}{8\pi^2} \left(\frac{4\pi}{Q^2} \right)^{\varepsilon} \frac{1}{\Gamma(1-\varepsilon)} \right) \int \mathrm{d}y_{13}\, \mathrm{d}y_{23} (y_{13} y_{23} (1 - y_{13} - y_{23}))^{-\varepsilon} \times \theta(1 - y_{13} - y_{23}), \tag{2.7}$$

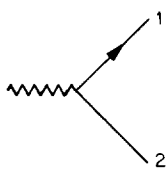

(a)

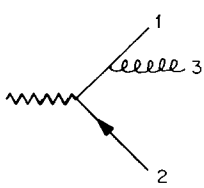

(b)

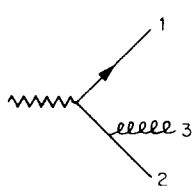

(c)

Fig. 2. (a) The reaction $\gamma^* \to q + \bar{q}$. (b, c) The reaction $\gamma^* \to q + \bar{q} + G$.

where

$$A_0 = \left(\frac{1}{2\pi} \frac{\Gamma(1-\varepsilon)}{\Gamma(2-2\varepsilon)} \left(\frac{4\pi}{Q^2} \right)^{\varepsilon} Q^2 \right).$$

The matrix elements are calculated as follows. The first step is to calculate the transition probability for a virtual photon of mass Q^2 to produce the various final states, eqs. (2.1)–(2.4). If we integrate over the angular correlations between the final state and the incoming beams, the summation over the polarizations of the incoming virtual photon may be replaced by $-g^{\mu\nu}$:

$$\sum_{\text{polarization}} \varepsilon^{\mu}(Q)\varepsilon^{\nu *}(Q) = -g^{\mu\nu}. \tag{2.8}$$

Explicit calculations of this matrix element and all other matrix elements in this paper are calculated in n dimensions using GAMALG [12] which is implemented in MACSYMA [13]. The result for the two-jet cross section, which defines our normalization is given by

$$\frac{1}{\sigma_0} \mathrm{d}\sigma^{(2)} = H \int \mathrm{d}y_{12}\, \delta(y_{12} - 1), \qquad H = 1 + \mathrm{O}(\varepsilon), \tag{2.9}$$

where

$$\sigma_0 = \frac{4\pi\alpha^2}{3Q^2} N_{\mathrm{C}} \sum_{k=1}^{n_{\mathrm{f}}} e_k^2$$

and $N_{\mathrm{C}} = 3$ is the number of colors, n_{f} is the number of flavors, e_k is the charge of the quark in units of the proton charge and H is a constant of proportionality equal to one in four dimensions.

From the three-jet diagrams of fig. 2 we obtain

$$\frac{1}{\sigma_0} \frac{\mathrm{d}\sigma^{(3)}}{\mathrm{d}s_{13}\,\mathrm{d}s_{23}} = H \frac{\alpha_{\mathrm{s}}}{2\pi} C_{\mathrm{F}} \left(\frac{4\pi\mu^2}{Q^2} \right)^{\varepsilon} \frac{1}{\Gamma(1-\varepsilon)} \frac{1}{Q^4} T(s_{12}, s_{13}, s_{23})$$

$$\times \theta\,(1 - y_{13} - y_{23})(y_{13}y_{23}(1 - y_{13} - y_{23}))^{-\varepsilon}, \tag{2.10}$$

where

$$T(s_{12}, s_{13}, s_{23}) = \left\{ \frac{(1-\varepsilon)s_{23}}{s_{13}} + \frac{(1-\varepsilon)s_{13}}{s_{23}} + \frac{2[\, s_{12}(s_{12} + s_{13} + s_{23}) - \varepsilon s_{13}s_{23}\,]}{s_{13}s_{23}} \right\}, \tag{2.11}$$

and μ is an arbitrary parameter with the dimensions of mass included to keep the

coupling constant dimensionless in n dimensions. From eq. (2.10) alone we can calculate $(1/\sigma_0)\mathrm{d}\sigma^{(3)}/\mathrm{d}C$ for all values of C except in the two-jet region ($C=0$) where there are infrared divergences. Setting $\varepsilon = 0$ and introducing the more usual variables $x_1 = 1 - y_{23}$, $x_2 = 1 - y_{13}$, we have

$$\frac{1}{\sigma_0}\frac{\mathrm{d}\sigma}{\mathrm{d}C} = \frac{\alpha_s}{2\pi} C_F \int_0^1 \mathrm{d}x_1 \int_0^1 \mathrm{d}x_2 \theta(x_1 + x_2 - 1) \frac{x_1^2 + x_2^2}{(1-x_1)(1-x_2)}$$

$$\times \delta\left(C - \frac{6(1-x_1)(1-x_2)(x_1+x_2-1)}{x_1 x_2 (2 - x_1 - x_2)} \right). \tag{2.12}$$

Performing the delta-function integration we obtain

$$\frac{1}{\sigma_0}\frac{\mathrm{d}\sigma^{(3)}}{\mathrm{d}C} = \frac{\alpha_s}{2\pi} C_F \int_{x_2^-(C)}^{x_2^+(C)} \mathrm{d}x$$

$$\times \frac{6x\left[C\left(x^3 + (x-2)^2\right) - 6(1-x)(1+x^2) \right]}{C(C+6)^2 (x - 6/(C+6))\sqrt{(6/(C+6) - x)(x_2^+ - x)(x - x_2^-)x}} \tag{2.13}$$

where

$$x_2^{\pm}(C) = \frac{1 + \frac{2}{3}C \pm \sqrt{1 - \frac{4}{3}C}}{\frac{1}{3}C + 2}. \tag{2.14}$$

From the above integral we can obtain the limiting asymptotic form around the three-jet value $C = \frac{3}{4}$:

$$\left.\frac{C}{\sigma_0}\frac{\mathrm{d}\sigma^{(3)}}{\mathrm{d}C}\right|_{C=3/4} = C_F \left(\frac{2^6 \pi}{3^3 \sqrt{3}} \right) \frac{\alpha_s}{2\pi} = 5.73 \frac{\alpha_s}{2\pi}. \tag{2.15}$$

A plot [4] of $(1/\sigma)\mathrm{d}\sigma^{(3)}/\mathrm{d}C$ is shown in fig. 3. This plot together with the information on the value of the total cross section through order (α_s) completely specifies the distribution. The whole C distribution can be computed by adding a delta function at the origin whose coefficient is such that the area under the curve is equal to the known perturbatively corrected total cross section. Employing the $\overline{\mathrm{MS}}$ subtraction scheme [14], this result for this quantity is given by [15, 16]

$$\frac{1}{\sigma_0}\sigma = 1 + \frac{\alpha_s(Q^2)}{2\pi}\left(\frac{3}{2}C_F\right) + \left(\frac{\alpha_s(Q^2)}{2\pi}\right)^2 \left[C_F\left(\tfrac{123}{8}N_C - \tfrac{3}{8}C_F - \tfrac{11}{2}T_R - 6\zeta(3)b_0\right)\right]$$

$$\equiv 1 + \frac{\alpha_s(Q^2)}{\pi} + \left(\frac{\alpha_s(Q^2)}{\pi}\right)^2 (1.986 - 0.115 n_f), \tag{2.16}$$

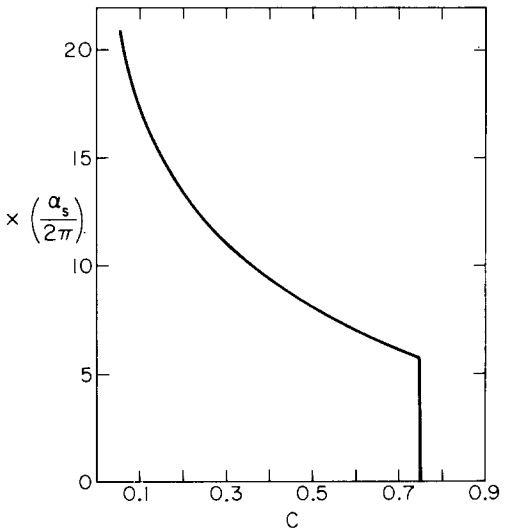

Fig. 3. Plot of $(C/\sigma_0)\,\mathrm{d}\sigma/\mathrm{d}C$ (in units of $\alpha_s/2\pi$) versus C.

where [17]

$$\frac{\alpha_s(Q^2)}{2\pi} = \frac{1}{b_0 \ln(Q^2/\Lambda^2) + (b_1/b_0)\ln(\ln(Q^2/\Lambda^2))},$$

$$\zeta(3) = 1.2021\,, \qquad b_0 = \tfrac{1}{6}(11N_C - 4T_R)\,, \qquad b_1 = \left(\tfrac{17}{6}N_C^2 - \tfrac{5}{3}N_C T_R - C_F T_R\right), \tag{2.17}$$

and the Casimir operators are $C_F = \frac{4}{3}$, $N_C = 3$, $T_R = \frac{1}{2}n_f$. At present we are interested only in the $O(\alpha_s)$ correction but we include the $O(\alpha_s^2)$ correction for later convenience.

The radiative corrections to the three gluon cross section are shown in fig. 4. In order α_s^2 they give contributions because of their interference with the lower-order diagrams of figs. 2b, c. To calculate the corrections we found it most efficient to square the amplitudes and perform the traces to reduce the transition probability to a Lorentz scalar, before integrating over the virtual gluon loop momentum l.

It is then convenient to shift numerator factors so that they cancel against denominators. For example, we rewrite

$$\frac{l\cdot p_2}{l^2(l-p_2)^2(l+p_3)^2(l+p_1+p_3)^2} \to \frac{1}{2(l-p_2)^2(l+p_3)^2(l+p_1+p_3)^2} - \frac{1}{2l^2(l+p_3)^2(l+p_1+p_3)^2}\,. \tag{2.18}$$

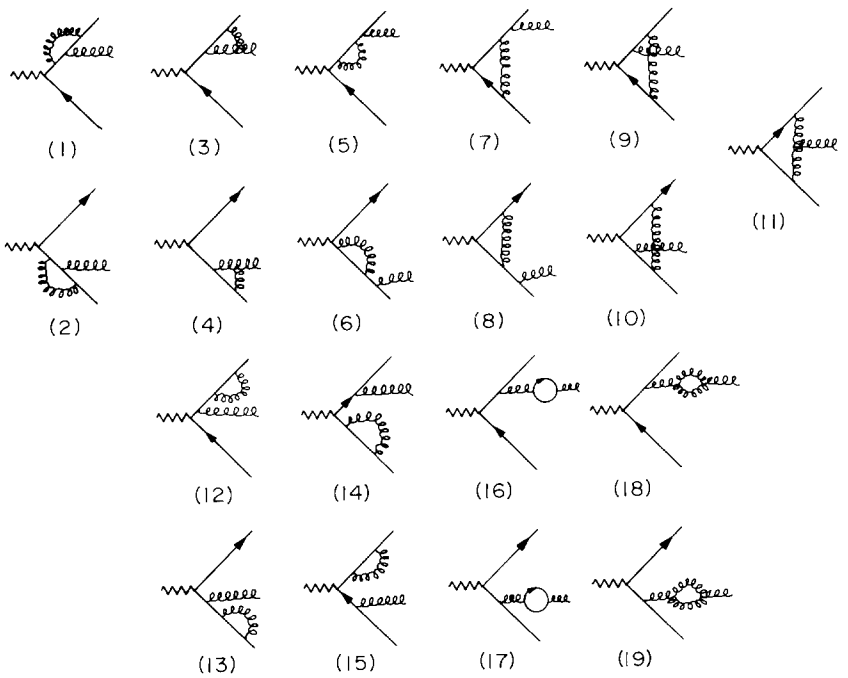

Fig. 4. Virtual corrections to the process $\gamma^*(Q) \to q + \bar{q} + G$. Diagrams 12 to 19 are contributions to wave function renormalization. Corrections to the gluon wave function involving ghosts or the four-gluon vertex and similar in structure to graphs 18 and 19 have not been shown.

By so doing we reduce the problem to a set of standard integrals involving fewer denominators and fewer powers of the loop momentum in the numerator. To aid the reader who wishes to check our results we have presented our results for certain integrals in appendix A.

We perform calculations in the Feynman gauge. As previously noted the ultraviolet divergences are controlled by dimensional regularization. We perform renormalization in the so-called $\overline{\text{MS}}$ scheme which corresponds to the subtraction of ultraviolet poles together with the attendant Euler-Mascheroni constant and $\ln 4\pi$. The $\overline{\text{MS}}$ counterterm is given by,

$$\frac{1}{\sigma_0}\mathrm{d}\sigma^{\mathrm{CT}} = H\left(\frac{\alpha_s}{2\pi}\right)C_F\left(\frac{4\pi\mu^2}{Q^2}\right)^{\varepsilon}\frac{1}{\Gamma(1-\varepsilon)}\frac{1}{Q^4}\int \mathrm{d}s_{13}\,\mathrm{d}s_{23}$$

$$\times T(Q^2 - s_{13} - s_{23}, s_{13}, s_{23})(y_{13}y_{23}(1 - y_{13} - y_{23}))^{-\varepsilon}$$

$$\times\left[\left(\frac{\alpha_s}{2\pi}\right)\frac{\Gamma(1-\varepsilon)}{\Gamma(1-2\varepsilon)}\left(\frac{4\pi\mu^2}{Q^2}\right)^{\varepsilon}\left(\tfrac{2}{3}T_R - \tfrac{11}{6}N_C\right)\left(\frac{1}{\varepsilon} + \ln\frac{Q^2}{\mu^2}\right) + O(\varepsilon)\right], \tag{2.19}$$

up to terms of order ε and higher which have been added so that eq. (2.19) can be cast in a convenient form. The function T, defined in eq. (2.11) gives the kinematic structure of the $O(\alpha_s)$ cross section.

In intermediate stages of the calculation the length of the expression becomes large, but the final result for the three-gluon cross section assumes the relatively simple form

$$\frac{1}{\sigma_0}\mathrm{d}\sigma^{(3)} = H\frac{\alpha_s(Q^2)}{2\pi}C_F\left(\frac{4\pi\mu^2}{Q^2}\right)^{\varepsilon}\frac{1}{\Gamma(1-\varepsilon)Q^4}\int \mathrm{d}s_{12}\,\mathrm{d}s_{13}\,\mathrm{d}s_{23}(y_{12}y_{13}y_{23})^{-\varepsilon}$$

$$\times\delta(Q^2 - s_{12} - s_{13} - s_{23})$$

$$\times\left\{T(s_{12},s_{13},s_{23})\left[1+\frac{\alpha_s}{2\pi}\frac{\Gamma(1-\varepsilon)}{\Gamma(1-2\varepsilon)}\left(\frac{4\pi\mu^2}{Q^2}\right)^{\varepsilon}\right.\right.$$

$$\left.\times\left(\frac{2C_F+N_C}{-\varepsilon^2}-\frac{1}{\varepsilon}\left(3C_F-2C_F\ln y_{12}+\tfrac{11}{6}N_C+N_C\ln\frac{y_{12}}{y_{13}y_{23}}-\tfrac{2}{3}T_R\right)\right)\right]$$

$$+\frac{\alpha_s}{2\pi}F(s_{12},s_{13},s_{23})$$

$$+\frac{\alpha_s}{2\pi}\left[T(s_{12},s_{13},s_{23})\left(\tfrac{2}{3}\pi^2\left(C_F+\tfrac{1}{2}N_C\right)-8C_F-C_F\ln^2 y_{12}\right.\right.$$

$$\left.\left.+\tfrac{1}{2}N_C(\ln^2 y_{12}-\ln^2 y_{13}-\ln^2 y_{23})\right)\right]\Bigg\}, \tag{2.20}$$

where the function F is defined as

$$F(s_{12},s_{13},s_{23}) = \left\{C_F\left[\frac{s_{12}}{s_{12}+s_{13}}+\frac{s_{12}}{s_{12}+s_{23}}+\frac{s_{12}+s_{23}}{s_{13}}+\frac{s_{12}+s_{13}}{s_{23}}\right]\right.$$

$$+\ln y_{13}\left[\frac{C_F(4s_{12}^2+2s_{12}s_{13}+4s_{12}s_{23}+s_{13}s_{23})}{(s_{12}+s_{23})^2}+\frac{N_C s_{13}}{s_{12}+s_{23}}\right]$$

$$+\ln y_{23}\left[\frac{C_F(4s_{12}^2+2s_{12}s_{23}+4s_{12}s_{13}+s_{13}s_{23})}{(s_{12}+s_{13})^2}+\frac{N_C s_{23}}{s_{12}+s_{13}}\right]$$

$$-2\left(C_F-\tfrac{1}{2}N_C\right)\Bigg[\frac{s_{12}^2+(s_{12}+s_{13})^2}{s_{13}s_{23}}R(y_{12},y_{23})+\frac{s_{12}^2+(s_{12}+s_{23})^2}{s_{13}s_{23}}R(y_{12},y_{13})$$

$$+\frac{Q^2(s_{13}^2+s_{23}^2)}{s_{13}s_{23}(s_{13}+s_{23})}-2\ln y_{12}\left(\frac{s_{12}^2}{(s_{13}+s_{23})^2}+\frac{2s_{12}}{s_{13}+s_{23}}\right)\Bigg]$$

$$-N_C T(s_{12},s_{13},s_{23})R(y_{13},y_{23})\Bigg\}, \tag{2.21}$$

and the function R is defined as

$$R(x,y)=\left[\ln x\ln y-\ln x\ln(1-x)-\ln y\ln(1-y)+\tfrac{1}{6}\pi^2-\mathrm{Li}_2(x)-\mathrm{Li}_2(y)\right], \tag{2.22}$$

where $\mathrm{Li}_2(x)$ is the normal dilogarithm function

$$\mathrm{Li}_2(x)=-\int_0^x\frac{\ln(1-z)}{z}\,\mathrm{d}z. \tag{2.23}$$

Several features of eq. (2.20) are worthy of note. Firstly, the coupling constant in eq. (2.20) is now the running coupling constant defined in the $\overline{\mathrm{MS}}$ scheme. Secondly, the divergent terms coming from the emission of soft and collinear radiation have the same form as the lowest-order cross section (modulo logarithms). Thirdly, we note the appearance of π^2 terms proportional to the lowest-order cross section which are intimately related to the soft singularity

$$\mathrm{Re}\left\{\left(\frac{4\pi\mu^2}{-Q^2}\right)^{\varepsilon}\left(-\frac{2}{\varepsilon^2}\right)\right\}=\left(\frac{4\pi\mu^2}{Q^2}\right)^{\varepsilon}\left(-\frac{2}{\varepsilon^2}+\pi^2\right)+\mathrm{O}(\varepsilon). \tag{2.24}$$

This concludes our discussion of the three-parton final state.

3. Calculation of diagrams involving four particles in the final state

The aim of this section is to present the calculation of diagrams with four partons in the final state, set up in such a way that the singularities which occur when a four-jet event masquerades as a three-jet event (i.e., the region of one soft

and/or collinear emission) can be easily extracted. Since we are interested in calculating a Lorentz invariant quantity, we are at liberty to evaluate different terms in the transition probability in different Lorentz frames.

For example, if we are interested in a term which contains the denominator s_{13}, it is convenient to set up the four-body phase space as a "quasi-three-body production"

$$\begin{array}{l} Q \to p_{13} + p_2 + p_4 \\ \qquad \hookrightarrow (p_1 + p_3) . \end{array} \tag{3.1}$$

We shall refer to this as the "1-3 system". To write down the four-particle phase space in this system we move to the c.m. frame of the produced composite,

$$p_1 = \tfrac{1}{2}\sqrt{s_{13}}\,(1, \ldots, \sin\theta\cos\theta', \cos\theta), \tag{3.2}$$

$$p_3 = \tfrac{1}{2}\sqrt{s_{13}}\,(1, \ldots, -\sin\theta\cos\theta', -\cos\theta), \tag{3.3}$$

$$p_2 = \frac{s_{123} - s_{13}}{2\sqrt{s_{13}}}(1, \ldots, 0, 1), \tag{3.4}$$

$$p_4 = \frac{s_{134} - s_{13}}{2\sqrt{s_{13}}}(1, \ldots, \sin\beta, \cos\beta), \tag{3.5}$$

where the dots in eqs. (3.2), (3.3) indicate $n-3$ unspecified, equal and opposite angles (in n dimensions) and $n-3$ zeros in eqs. (3.4), (3.5). Four-momentum conservation constrains $\cos\beta$:

$$\tfrac{1}{2}(1 - \cos\beta) = \frac{s_{13}(Q^2 - s_{123} - s_{134} + s_{13})}{(s_{123} - s_{13})(s_{134} - s_{13})} . \tag{3.6}$$

Setting $v = \frac{1}{2}(1 - \cos\theta)$, we obtain for the n-dimensional phase space in this system:

$$\begin{aligned} (\mathrm{PS})^{(4)} = A_0 \Bigg\{ \left(\frac{1}{8\pi^2} \left(\frac{4\pi}{Q^2} \right)^{\varepsilon} \frac{1}{\Gamma(1-\varepsilon)} \right)^2 \tfrac{1}{16} S Q^2 \Bigg[\int \mathrm{d}y_{123}\, \mathrm{d}y_{134}\, \mathrm{d}y_{13} (y_{123} y_{134} - y_{13})^{-\varepsilon} \\ \times (y_{13} + 1 - y_{123} - y_{134})^{-\varepsilon} (y_{13})^{-\varepsilon} \theta(y_{13}) \theta(y_{123} y_{134} - y_{13}) \\ \times \theta(y_{13} + 1 - y_{123} - y_{134}) \times \int_0^1 \mathrm{d}v (v(1-v))^{-\varepsilon} \frac{1}{N_{\theta'}} \int_0^{\pi} \mathrm{d}\theta' \sin^{-2\varepsilon}\theta' \Bigg] \Bigg\} . \end{aligned} \tag{3.7}$$

A_0 is given in eq. (2.7), S is the statistical factor and $N_{\theta'}$ is a normalization factor determined such that

$$\int_0^\pi \mathrm{d}\theta' \sin^{-2\varepsilon}\theta' = N_{\theta'} = 2^{2\varepsilon}\pi \frac{\Gamma(1-2\varepsilon)}{\Gamma^2(1-\varepsilon)} . \tag{3.8}$$

After integration over θ' and v, the angular distribution of the produced composite s_{13}, the form of the phase-space distribution is very similar to the three-particle phase space [eq. (2.7)], except for the differing range of integration. The lower limit of the y_{13} integration is specified by the θ functions

$$\theta(y_{13})\theta(y_{13}+1-y_{123}-y_{134}) \to \theta(y_{13})\theta(1-y_{123}-y_{134}) + \theta(y_{123}+y_{134}-1)\theta(y_{13}+1-y_{123}-y_{134}),$$

so the range of the s_{13} integration is split so that

$$\int \mathrm{d}y_{13} \to \theta(1-y_{123}-y_{134}) \int_0^{y_{123}y_{134}} \mathrm{d}y_{13} + \theta(y_{123}+y_{134}-1) \int_{y_{123}+y_{134}-1}^{y_{123}y_{134}} \mathrm{d}y_{13} .$$

A term containing a denominator s_{13} will give a singularity only in the first region of integration. The structure of this first region of integration when substituted into eq. (3.7) is exactly analogous to eq. (2.7). Possible divergences resulting from the emission of parton 3 collinear and/or soft with respect to parton 1 are associated with the integrations over s_{13}, v and θ' in the first region of s_{13} integration.

The calculation of the transition probability for the process

$$\gamma^*(Q) \to \mathrm{q}(p_1) + \bar{\mathrm{q}}(p_2) + \mathrm{G}(p_3) + \mathrm{G}(p_4) \tag{3.9}$$

from the eight diagrams shown in fig. 5 contains in principle 36 terms. Many of them are related by interchange of momentum labels and, in all, only 13 transition probabilities need be calculated. In table 1 we give the momentum label interchanges necessary to generate all the transition probabilities from the thirteen which we choose to calculate. The interference of graph Bi with Bj is written as Bij, $(i \geqslant j)$.

It is therefore sufficient to consider the thirteen transition probabilities on the top row of table 1, which we display in fig. 6. The on-shell partons are denoted by the cutting lines and the numbers refer to the labels of the external legs. The transition probabilities are seen to fall into three classes:

(a) planar QED type graphs with group weight C_F^2;

(b) non-planar QED type graphs with group weight $C_F(C_F - \frac{1}{2}N_C)$;

(c) QCD graphs involving the three-gluon vertex with group weight $C_F N_C$.

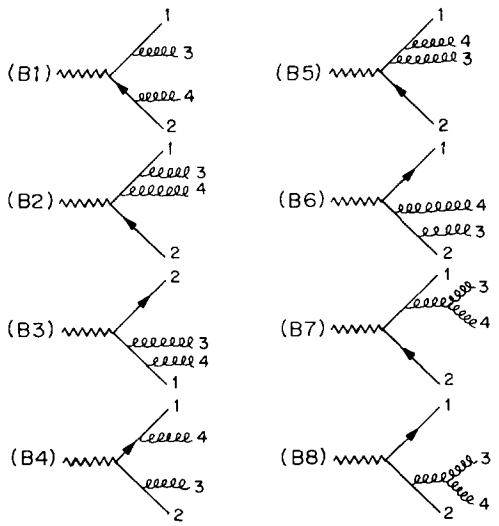

Fig. 5. Diagrams contributing to the process $\gamma^* \to q\bar{q}GG$.

All matrix elements are generated in n dimensions using GAMALG. We sum over the two physical polarizations of the produced gluons. This is most easily accomplished by summing over the polarizations with

$$\sum_{\text{pol}} \varepsilon^{\mu *} \varepsilon^{\nu} = -g^{\mu\nu}, \tag{3.10}$$

but including "ghost loop graphs" in diagrams B77, B87 (and B88) to take account of the fact that the gluon current is not conserved.

Our method of calculation of the event shape parameter C depends crucially on our ability to divide the transition probabilities into pieces which are divergent in

TABLE 1
The interchange table relating the graphs for $e^+e^- \to q\bar{q}GG$

Permutation of first row \ Group weight	Class A C_F^2				Class B $C_F(C_F - \frac{1}{2}N_C)$				Class C $C_F N_C$				
	B11	B32	B21	B22	B42	B52	B53	B41	B71	B72	B82	B77	B87
(3↔4)	B44	B65	B54	B55	B51		B62		B74	B75	B85		
(1↔2)			B64	B66	B61				B84	B86	B76	B88	
(1↔2), (3↔4)			B31	B33	B43	B63			B81	B83	B73		

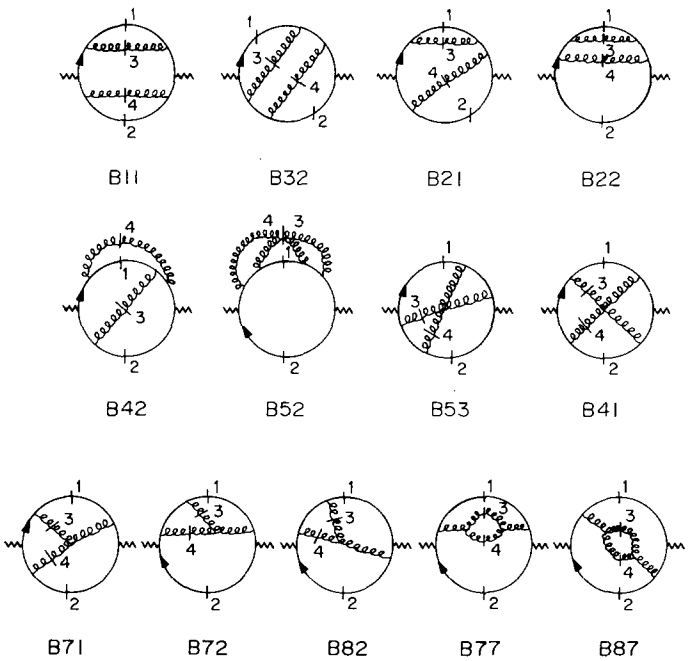

Fig. 6. Transition probabilities for the process $\gamma^* \to q\bar{q}GG$. On-shell particles are indicated by the short cutting line and the numbers refer to the momentum labels. All the other transition probabilities can be obtained by permutation of momentum labels.

the three-jet region when a *single* denominator from the set s_{13}, s_{23}, s_{14}, s_{24}, or s_{34} vanishes. This is clearly always possible since the vanishing, for example, of s_{13} corresponds to the region in which gluon p_3 is collinear and/or soft with respect to quark p_1. In the Feynman gauge [cf. eq. (3.10)] (and in all but physical gauges) a particular diagram contains overlapping infrared divergences. Individual graphs diverge as any one of several s_{ij}'s vanishes, reflecting the fact that it may be made to simulate a three-jet diagram in several different ways. We divide each graph into pieces which only contain singularities as a single s_{ij} vanishes. These various pieces correspond to the different ways that a four-parton final state can assume a three-jet structure because of the coalescence of two partons.

Two examples will clarify our procedure. Suppressing numerator factors, graph B52 (fig. 6) may be written as

$$\mathrm{B52} \sim \frac{1}{s_{134}^2 s_{13} s_{14}} . \tag{3.11}$$

The potentially dangerous terms in eq. (3.11) are s_{13} and s_{14}, since s_{134} can vanish only in the two-jet configuration in which partons 1, 3 and 4 recoil against parton

2. Partial fractioning eq. (3.11), we get

$$\mathrm{B52} \sim \frac{1}{s_{134}^2 s_{13}(s_{13}+s_{14})} + \frac{1}{s_{134}^2 s_{14}(s_{13}+s_{14})} . \tag{3.12}$$

The first term in eq. (3.12) should be calculated in the "1-3 system", eqs. (3.2)–(3.5). In this system s_{134} is one of the subsequent variables of integration and hence for the purposes of the s_{13} integration it is held fixed. Both denominators s_{13} and $(s_{13}+s_{14})$ may vanish (at fixed s_{134} and s_{123}) but the latter only when s_{13} also vanishes, since s_{13} and s_{14} are both positive semidefinite

$$(s_{13}+s_{14}) \to 0 , \qquad (s_{13}=0, \cos\theta = 1) . \tag{3.13}$$

The treatment of the second term in eq. (3.12) is identical in the "1-4 system".

Partial fractioning similar to the above must be applied throughout. For example, suppressing most of the numerator, graph B41 (fig. 6) is given by,

$$\mathrm{B41} \sim \frac{s_{12}}{s_{13}s_{14}s_{23}s_{24}} . \tag{3.14}$$

Performing successive partial fractioning we rewrite this term as

$$\frac{s_{12}}{s_{13}s_{14}s_{23}s_{24}} \equiv \left[\frac{s_{12}}{(s_{24}-s_{13})(s_{13}+s_{14})(s_{13}+s_{23})s_{13}} + (3\leftrightarrow 4) + (1\leftrightarrow 2) + (3\leftrightarrow 4, 1\leftrightarrow 2) \right] . \tag{3.15}$$

The first term in eq. (3.15) (written out explicitly) is singular as $s_{13}\to 0$. In the "1-3 system" we may write its singular part,

$$\frac{s_{12}}{(s_{24}-s_{13})(s_{13}+s_{14})(s_{13}+s_{23})s_{13}} \underset{\text{fixed } s_{123}, s_{134}}{\overset{s_{13}\to 0}{\to}} \frac{s_{123}}{(Q^2 - s_{123} - s_{134})s_{134}(s_{13}v + s_{123}(1-v))s_{13}} . \tag{3.16}$$

The right-hand side of eq. (3.16) contains two denominators singular in the three-jet region but both require the vanishing of s_{13}. For this argument the presence of the s_{12} factor in the numerator is essential. In the "1-3 system" when s_{13} vanishes partons 2 and 4 are parallel so that s_{12} and s_{14} are proportional to one another. The constant of proportionality depends only on the variables s_{123} and s_{134}

which are kept fixed during the s_{13} integration. Hence in the singular limit $s_{12}/(s_{13}+s_{14})$ is replaced by a constant. The denominators s_{134} and $(Q^2-s_{123}-s_{134})$ can also vanish but only in the two-jet region $C=0$.

Our calculation procedure is as follows. We first calculate all the transition probabilities in n dimensions. The full result for $d\sigma^{(4)}$ in four dimensions is given in appendix B. We then partial fraction, as described in the previous paragraph so that the resultant pieces are divergent in the three-jet region only when a single s_{ij} vanishes. We then collect together all the terms corresponding to the various s_{ij}. The answers fall into different pieces identified by differing group weight factors. Here we present the singular parts of these terms in the three-jet region for spacetime dimensionality $n=4-2\varepsilon$. After integration the singularities of these pieces will explicitly cancel against the poles in the virtual diagrams [eq. (2.20)].

The part of the four-parton cross section which is singular when a quark and a gluon are collinear (or soft) with respect to one another is given by*

$$\begin{aligned}
\frac{1}{\sigma_0}\,d\sigma_1^{(s)} = H\frac{\alpha_s}{2\pi}C_F\left(\frac{4\pi\mu^2}{Q^2}\right)^{\varepsilon}\frac{1}{\Gamma(1-\varepsilon)}\frac{1}{Q^4}
\\ \times\Bigg[\Bigg\{\int ds_{123}\,ds_{134}\,ds_{13}(y_{123}y_{134})^{-\varepsilon}(1-y_{123}-y_{134})^{-\varepsilon}(y_{13})^{-\varepsilon}
\\ \times\theta(y_{13})\theta(y_{123}y_{134}-y_{13})\theta(1-y_{123}-y_{134})\int_0^1 dv(v(1-v))^{-\varepsilon}\frac{1}{N_{\theta'}}
\\ \times\int_0^{\pi} d\theta'\sin^{-2\varepsilon}\theta'\times\frac{1}{2}\frac{\alpha_s}{2\pi}\left(\frac{4\pi\mu^2}{Q^2}\right)^{\varepsilon}\frac{1}{\Gamma(1-\varepsilon)}\frac{T(s_{123},s_{134},Q^2-s_{123}-s_{134})}{s_{13}}
\\ \times\Bigg[C_F\left(\frac{2s_{123}}{s_{13}v+s_{123}(1-v)}-1-v-\varepsilon(1-v)\right)
\\ +N_C\left(\frac{s_{134}}{s_{13}+s_{34}}-\frac{s_{123}}{s_{13}+s_{23}}\right)\Bigg]\Bigg\}
\\ +\{(3\leftrightarrow 4)\}+\{(1\leftrightarrow 2)\}+\{(1\leftrightarrow 2,3\leftrightarrow 4)\}\Bigg],
\end{aligned}\tag{3.17}$$

and the function T is given in eq. (2.11). The above formula is to be interpreted with v and θ' transforming under the indicated interchanges. Under $(3\leftrightarrow 4)$

* In the following equations we have dropped integrable square root singularities.

interchange (i.e., transforming from the "1-3 system" to the "1-4 system") we have

$$v = \frac{s_{12}}{s_{12}+s_{23}} \to \tilde{v} = \frac{s_{12}}{s_{12}+s_{24}},$$

$$(1-\sin\theta\cos\theta'\sin\beta-\cos\theta\cos\beta) = \frac{s_{14}}{s_{14}+s_{34}} \to \frac{s_{13}}{s_{13}+s_{34}}$$

$$= (1-\sin\tilde{\theta}\cos\tilde{\theta}'\sin\tilde{\beta}-\cos\tilde{\theta}\cos\tilde{\beta}), \tag{3.18}$$

and similarly for the other interchanges. Several features of eq. (3.17) should be noted. Firstly it has the kinematic structure of the $O(\alpha_s)$ matrix element. It is proportional to the matrix element squared T in which particles one and three (or the other interchanges) are considered as a single composite. Also the coefficient of the s_{13} singularity proportional to C_F may be written for $v \neq 1$ as

$$P_{qq}^{n\neq 4}(v) = C_F\left(\frac{2}{1-v} - 1 - v - \varepsilon(1-v)\right),$$

which is seen to be the generalization to n dimensions of the Altarelli-Parisi function [18]. The other singular contributions in eq. (3.17) are proportional to N_C. These are terms, which are singular in the three-jet region but make no contribution, in the leading log approximation. They are therefore not related to Altarelli-Parisi kernels. The existence of these terms indicates that the leading log approximation may not be used to extract information about subleading logs.

The other terms proportional to the N_C are singular in the limit when a pair of gluons become collinear and/or parallel. Their contribution is

$$\frac{1}{\sigma_0}\mathrm{d}\sigma_{II}^{(s)} = H\frac{\alpha_s}{2\pi}C_F\left(\frac{4\pi\mu^2}{Q^2}\right)^{\varepsilon}\frac{1}{\Gamma(1-\varepsilon)}\frac{1}{Q^4}$$

$$\times\int \mathrm{d}s_{134}\,\mathrm{d}s_{234}\,\mathrm{d}s_{34}(y_{134}y_{234})^{-\varepsilon}(1-y_{134}-y_{234})^{-\varepsilon}(y_{34})^{-\varepsilon}$$

$$\times\theta(y_{34})\theta(y_{134}y_{234}-y_{34})\theta(1-y_{134}-y_{234})\int_0^1 \mathrm{d}v(v(1-v))^{-\varepsilon}\frac{1}{N_{\theta'}}$$

$$\times\int_0^{\pi}\mathrm{d}\theta'\sin^{-2\varepsilon}\theta'$$

$$\times\frac{1}{2}\frac{\alpha_s}{2\pi}\left(\frac{4\pi\mu^2}{Q^2}\right)^{\varepsilon}\frac{1}{\Gamma(1-\varepsilon)}\frac{N_C}{s_{34}}$$

$$\times \Bigg\{ T(Q^2 - s_{134} - s_{234}, s_{134}, s_{234}) \times \left[\frac{s_{234}}{s_{34}+s_{23}} + \frac{s_{234}}{s_{34}+s_{24}} + \frac{s_{134}}{s_{34}+s_{13}} + \frac{s_{134}}{s_{34}+s_{14}} - 4 + 2v(1-v) \right] + \left(2(1-\varepsilon)\cos^2\theta' - 1\right) 4v(1-v) \frac{Q^2(Q^2 - s_{134} - s_{234})}{s_{134}s_{234}} \Bigg\}. \tag{3.19}$$

Here again the result has the kinematic structure of the lowest order with partons 3 and 4 interpreted as a single particle (plus terms which vanish after integration over θ'). In this formula θ' and v are the angles appropriate to the "3-4 system"*. To check our results we note that after integration over θ' for $v \neq 0, 1$ we obtain the Altarelli-Parisi kernel [18]

$$P_{GG}(v) = N_C \left[\frac{2}{v} + \frac{2}{1-v} - 4 + 2v(1-v) \right]. \tag{3.20}$$

This kernel is unchanged in n dimensions.

Lastly we calculate the matrix elements for the process

$$\gamma^*(Q) \to \bar{q}(p_1) + \bar{q}(p_2) + q(p_3) + q(p_4), \tag{3.21}$$

from the diagrams shown in fig. 7. Only twelve of the possible thirty-six transition probabilities are independent. In table 2 we display the interchanges necessary to recover all the transition probabilities from the twelve which we choose to calculate. These twelve transition probabilities are shown graphically in fig. 8 where the cutting lines indicate the particles which are on-shell. The diagrams clearly fall into three classes distinguished by their group weight factors. Diagrams A81, A82, and A53 together with their companions generated by interchange (class F) give no contribution in an experiment in which the charge of the final particles is not detected. This is a consequence of charge conjugation—the non-abelian generalization of Furry's theorem [19]. The matrix elements for the remaining two classes (D and E) are given in four dimensions in appendix B. Here we quote only the pieces

* In our notation this corresponds to the interchanges $1 \to 3$, $3 \to 4$, $2 \to 1$, $4 \to 2$ in eqs. (3.2)–(3.5).

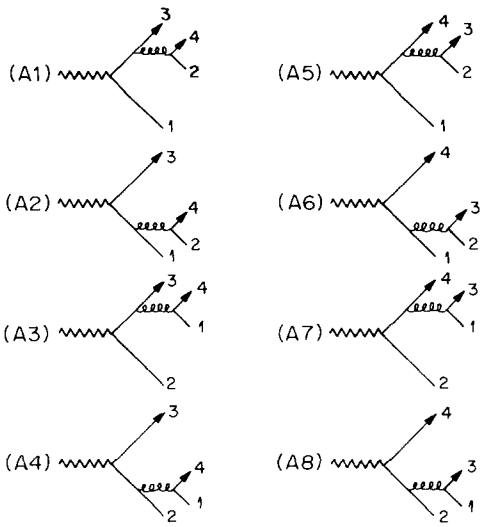

Fig. 7. Diagrams contributing to the process $\gamma^* \to q\bar{q}\,q\bar{q}$. Diagrams which differ only by the exchange of identical final state fermions have a relative minus sign.

TABLE 2
The interchange table relating the graphs for $e^+e^- \to \bar{q}\bar{q}qq$

Permutation of first row / Group weight	Class D $C_F T_R$			Class E $C_F(C_F - \frac{1}{2}N_C)$						Class F C_F		
	A77	A88	A87	A83	A76	A73	A86	A84	A75	A81	A82	A53
(1↔2)	A55	A66	A65	A61	A85	A51		A62		A63	A64	A71
(3↔4)	A33	A44	A43	A74	A32		A42		A31	A54		
(1↔2), (3↔4)	A11	A22	A21	A52	A41					A72		

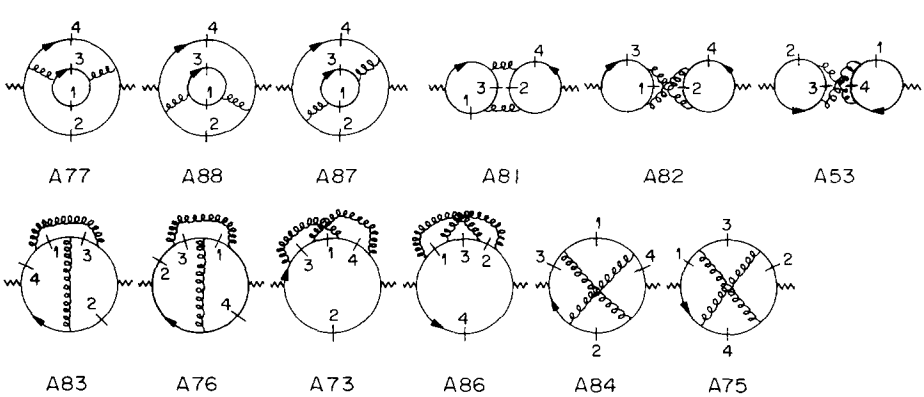

Fig. 8. Transition probabilities for the process $\gamma^* \to q\bar{q}\,q\bar{q}$. On-shell particles are indicated by a short cutting line and the numbers refer to the momentum labels. All other transition probabilities can be obtained by exchange of momentum labels.

singular in the three-jet region, in n dimensions,

$$\frac{1}{\sigma_0}\mathrm{d}\sigma_{\mathrm{III}}^{(s)} = H\frac{\alpha_s}{2\pi}C_F\left(\frac{4\pi\mu^2}{Q^2}\right)^{\varepsilon}\frac{1}{\Gamma(1-\varepsilon)}\frac{1}{Q^4}$$

$$\times\left\{\int \mathrm{d}s_{123}\,\mathrm{d}s_{134}\,\mathrm{d}s_{13}[(y_{123}y_{134})(1-y_{123}-y_{134})y_{13}]^{-\varepsilon}\right.$$

$$\times\theta(y_{13})\theta(y_{123}y_{134}-y_{13})\theta(1-y_{123}-y_{134})\int_0^1 \mathrm{d}v(v(1-v))^{-\varepsilon}\frac{1}{N_{\theta'}}$$

$$\times\int_0^{\pi}\mathrm{d}\theta'\sin^{-2\varepsilon}\theta'\times\frac{1}{4}\frac{\alpha_s}{2\pi}\left(\frac{4\pi\mu^2}{Q^2}\right)^{\varepsilon}\frac{1}{\Gamma(1-\varepsilon)}\frac{T_R}{s_{13}}$$

$$\times\left[T(Q^2-s_{123}-s_{134},s_{123},s_{134})\left(\frac{v^2+(1-v)^2-\varepsilon}{1-\varepsilon}\right)\right.$$

$$\left.\left.-\frac{Q^2(Q^2-s_{123}-s_{134})}{s_{123}s_{134}}4v(1-v)\left(2\cos^2\theta'-\frac{1}{(1-\varepsilon)}\right)\right]\right\}$$

$$+\{(1\leftrightarrow 2)\}+\{(3\leftrightarrow 4)\}+\{(1\leftrightarrow 2)(3\leftrightarrow 4)\}\,. \tag{3.22}$$

As a check on this result we notice that after integration over θ' the coefficient of the s_{13} pole is proportional to

$$P_{qG}^{n\neq 4}(v) = T_R\left(\frac{(v^2+(1-v)^2-\varepsilon)}{(1-\varepsilon)}\right), \tag{3.23}$$

which reduces to the normal Altarelli-Parisi [18] function in the limit $\varepsilon\to 0$.

Eqs. (3.17), (3.19) and (3.22) contain the singular part of the four-parton cross section as we approach the three-jet region. We therefore define

$$\mathrm{d}\sigma^{(s)} = \mathrm{d}\sigma_{\mathrm{I+II+III}}^{(s)}\,. \tag{3.24}$$

The two quantities in eq. (1.21) are now fully defined. Performing the first three integrations* in all the parts of eq. (3.24) and changing the names of the variables,

* This is permissible because $C^{(3)}$ in the delta function is independent of these variables and therefore gives no constraint.

we may write*

$$\frac{1}{\sigma_0}\mathrm{d}\sigma^{(s)} = H\frac{\alpha_s}{2\pi}C_F\left(\frac{4\pi\mu^2}{Q^2}\right)^{\epsilon}\frac{1}{\Gamma(1-\epsilon)}\frac{1}{Q^4}\int \mathrm{d}s_{12}\,\mathrm{d}s_{13}\,\mathrm{d}s_{23}(y_{12}y_{13}y_{23})^{-\epsilon}$$

$$\times\delta(Q^2-s_{12}-s_{13}-s_{23})T(s_{12},s_{13},s_{23})\frac{\alpha_s}{2\pi}\frac{\Gamma(1-\epsilon)}{\Gamma(1-2\epsilon)}\left(\frac{4\pi\mu^2}{Q^2}\right)^{\epsilon}$$

$$\times\left\{\frac{1}{\epsilon^2}(2C_F+N_C)+\frac{1}{\epsilon}\left(3C_F-2C_F\ln y_{12}+\tfrac{11}{6}N_C+N_C\ln\frac{y_{12}}{y_{13}y_{23}}-\frac{2}{3}T_R\right)\right.$$

$$+C_F\big[\ln^2 y_{12}-\ln^2 y_{13}-\ln^2 y_{23}-2\mathrm{Li}_2(1-y_{13})-2\mathrm{Li}_2(1-y_{23})+7$$

$$-3\ln y_{12}-\tfrac{3}{2}\ln y_{13}-\tfrac{3}{2}\ln y_{23}\big]$$

$$\times N_C\big[-\tfrac{3}{2}\ln^2 y_{12}+\tfrac{1}{2}\ln^2 y_{13}+\tfrac{1}{2}\ln^2 y_{23}-2\mathrm{Li}_2(1-y_{12})+\tfrac{67}{18}-\tfrac{11}{6}\ln y_{13}-\tfrac{11}{6}\ln y_{23}\big]$$

$$\left.\times T_R\big[\left(\tfrac{2}{3}\ln y_{13}+\tfrac{2}{3}\ln y_{23}-\tfrac{10}{9}\right)\big]\right\}. \tag{3.25}$$

Adding this to eq. (2.20), we obtain

$$\frac{1}{\sigma_0}\frac{\mathrm{d}\sigma^{(s)}+\mathrm{d}\sigma^{(3)}}{\mathrm{d}C}=\frac{\alpha_s(Q^2)}{2\pi}C_F\frac{1}{Q^4}\int \mathrm{d}s_{12}\,\mathrm{d}s_{13}\,\mathrm{d}s_{23}\,\delta(1-y_{12}-y_{13}-y_{23})$$

$$\times\delta\big(C-C^{(3)}(s_{12},s_{13},s_{23})\big)$$

$$\times\left\{T(s_{12},s_{13},s_{23})\Big[1+\frac{\alpha_s}{2\pi}C_F\left(\tfrac{2}{3}\pi^2-1-\ln^2 y_{13}-\ln^2 y_{23}-2\mathrm{Li}_2(1-y_{13})\right.\right.$$

$$-2\mathrm{Li}_2(1-y_{23})-3\ln y_{12}-\tfrac{3}{2}\ln y_{13}-\tfrac{3}{2}\ln y_{23}\big)$$

$$+\frac{\alpha_s}{2\pi}N_C\big(\tfrac{1}{3}\pi^2-\ln^2 y_{12}-2\mathrm{Li}_2(1-y_{12})$$

$$\left.+\tfrac{67}{18}-\tfrac{11}{6}\ln y_{13}-\tfrac{11}{6}\ln y_{23}\big)+\frac{\alpha_s}{2\pi}T_R\big(\tfrac{2}{3}(\ln y_{13}+\ln y_{23})-\tfrac{10}{9}\big)\Big]\right.$$

$$\left.+\frac{\alpha_s}{2\pi}F(s_{12},s_{13},s_{23})\right\}, \tag{3.26}$$

* One of the integrals required is given in appendix A.

where the function F is given in eq. (2.21). All poles have vanished in eq. (3.26) as they must and the limit $\varepsilon \to 0$ has been taken. Eq. (3.26) can be evaluated by a simple numerical integration. The full C distribution is given by the sum of eq. (3.26) and the term,

$$\frac{1}{\sigma_0} \mathrm{d}\sigma^{(4)} \delta(C - C^{(4)}) - \mathrm{d}\sigma^{(s)} \delta(C - C^{(3)}) . \tag{3.27}$$

Eq. (3.27) is completely finite except at $C = 0$ and hence may be evaluated in four dimensions. In sect. 4 the numerical values of the distributions of the C and D distributions are discussed.

4. Results

The numerical integration of the terms in eqs. (3.26) and (3.27) are treated separately since eq. (3.26) is a two-dimensional integration, (which we performed by ordinary numerical integration), whereas eq. (3.27) requires integration over five parameters and was integrated using a Monte Carlo technique which we describe below.

It was not practical to invert the expression for $C^{(4)}$ to use the delta function to eliminate one of the variables of integration. We therefore generated events, calculated the cross sections $\mathrm{d}\sigma^{(4)}$ and $\mathrm{d}\sigma^{(s)}$ and binned them according to their values of $C^{(4)}$ and $C^{(3)}$, respectively. In general, the bins $C^{(4)}$ and $C^{(3)}$ do not coincide. However, in the infrared limit where four-jet events simulate three-jet events

$$C^{(4)} \overset{s_{ij} \to 0}{\to} C^{(3)} + \mathrm{O}\left(s_{ij}^{1/2}\right) \tag{4.1}$$

[c.f., eq. (1.15)], so that in this region $\mathrm{d}\sigma^{(4)}$ and its singular part $\mathrm{d}\sigma^{(s)}$ are guaranteed to fall in the same bin and hence cancel. The approach of $C^{(4)}$ to $C^{(3)}$ is slow. Moreover $\mathrm{d}\sigma^{(4)}$ and $\mathrm{d}\sigma^{(s)}$ have double poles. There exist regions of phase space for which $C^{(4)}$ and $C^{(3)}$ lie in adjacent bins but where $\mathrm{d}\sigma^{(4)}$ and $\mathrm{d}\sigma^{(s)}$ are still large, thus adding a large contribution of one sign to one bin and a large contribution of the other sign to an adjacent bin. This causes fluctuations in our histograms which gradually decrease as the number of points is increased. Despite the fact that for the parts of the cross section which contain double poles, over 10^6 points were taken, remnants of these fluctuations can be seen in our histograms.

In figs. 9, 10, 11 we present our results* for the quantity $(C/\sigma)\,\mathrm{d}\sigma/\mathrm{d}C$ for the group weights $C_F N_C$, $C_F T_R$ and C_F^2, respectively. All three distributions display a

* In these plots σ is the total cross section, eq. (2.16) corrected to order α_s (and not σ_0).

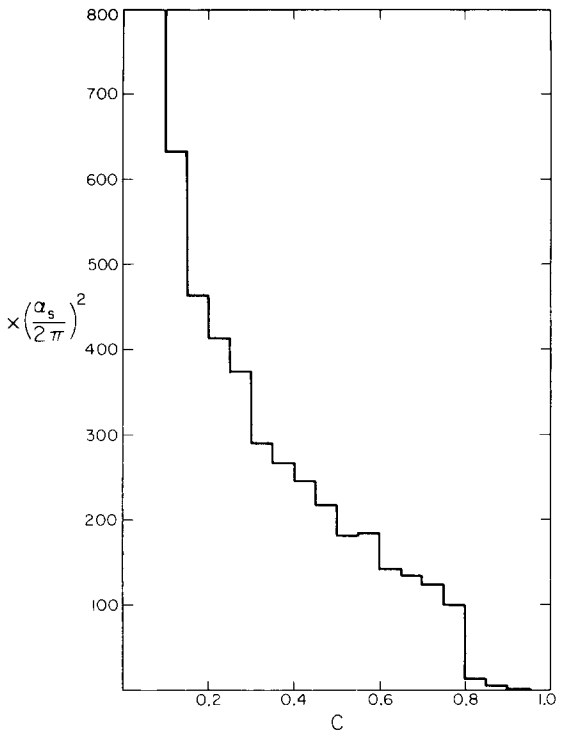

Fig. 9. The part of the $O(\alpha_s^2)$ correction to $(C/\sigma)\,d\sigma/dC$ containing the Casimirs $C_F N_C$ is plotted in units of $(\alpha_s/2\pi)^2$ against the variable C.

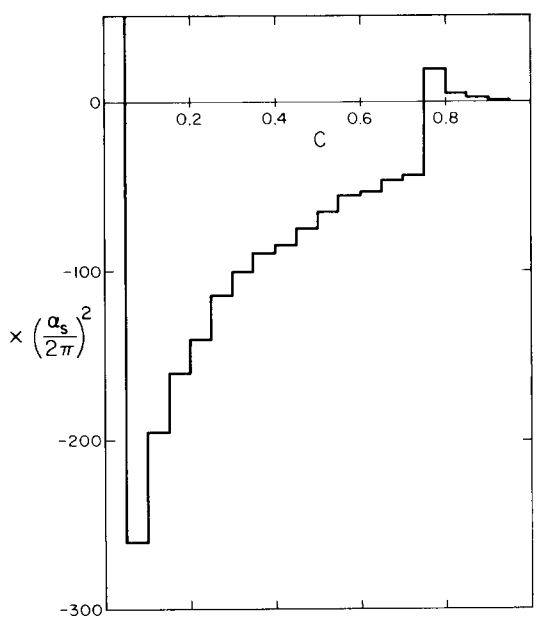

Fig. 10. The part of the $O(\alpha_s^2)$ correction to $(C/\sigma)\,d\sigma/dC$ containing the Casimirs $C_F T_R$ is plotted in units of $(\alpha_s/2\pi)^2$ against the variable C. The number of flavors is set equal to 5.

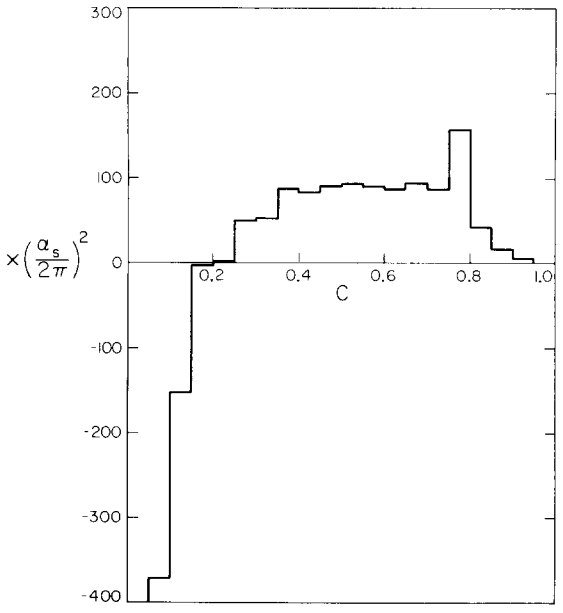

Fig. 11. The part of the $O(\alpha_s^2)$ correction to $(C/\sigma)\,d\sigma/dC$ containing the Casimirs C_F^2 is plotted in units of $(\alpha_s/2\pi)^2$ against the variable C.

discontinuity at $C=\frac{3}{4}$. Above $C=\frac{3}{4}$ the differential cross section receives contributions from $d\sigma^{(4)}$ only; these contributions diverge as $C\to\frac{3}{4}$ from above, as we approach the point where four jets coalesce to three. At the point $C=\frac{3}{4}$ and for all points $C<\frac{3}{4}$ this divergence is cancelled by $d\sigma^{(s)}$. For $C>\frac{3}{4}$ the cross section is constrained to be positive; for $C<\frac{3}{4}$ the distributions, figs. 9, 10, 11, are higher-order corrections to the lower-order distribution, fig. 3, and may therefore be negative as in fig. 10. The leading log behavior [c.f., eq. (3.26)] around $C=0$ [8, 20] is visible in fig. 11:

$$\frac{d\sigma}{dC}\bigg|_{\sim}\frac{\alpha_s}{2\pi}\frac{\ln C}{C}\left(1-\frac{\alpha_s}{2\pi}2C_F\ln^2 C\right). \tag{4.2}$$

However, by comparison with figs. 9, 10, we see that only at extremely low values of C is this leading log behavior the dominant effect. We have no way of calculating the distribution in the first bin since it contains divergences which are cancelled by the $O(\alpha_s^2)$ contributions to two-jet processes (proportional to a delta function at the origin). We can use the total cross section [15, 16], now known up to $O(\alpha_s^2)$, to calculate what the average value in this bin should be. Since the correction to the total cross section is small, but the correction for $C>0.05$ is large, a sizeable negative contribution is required in the first bin to balance it.

From our figures we can calculate the fraction of events which lie in the range $\frac{1}{2}<C<1$. This gives a measure of the multijet events (see fig. 1). Our numerical

estimate is

$$\frac{1}{\sigma}\int_{1/2}^{1}\frac{\mathrm{d}\sigma}{\mathrm{d}C}\,\mathrm{d}C = 2.8\left(\frac{\alpha_s(Q^2)}{2\pi}\right)\left[1+K\left(\frac{\alpha_s(Q^2)}{2\pi}\right)\right], \tag{4.3}$$

where

$$K = 36.5 \pm 0.5\,. \tag{4.4}$$

By choosing the range $\frac{1}{2} \leqslant C \leqslant 1$ we have excluded the pure two-jet region and also the perturbative two-jet events which are promoted to higher values of C by hadronization. Choosing a notional value of

$$\frac{\alpha_s(Q^2)}{2\pi} \sim 0.03\,, \qquad Q = 30\ \mathrm{GeV}\,, \qquad \Lambda = 0.5\ \mathrm{GeV}\,, \tag{4.5}$$

we see that the perturbation series in eq. (4.5) does not appear to converge.

Our conclusion is that the multijet fraction of e^+e^- hadronic events calculated in the $\overline{\mathrm{MS}}$ renormalization prescription does not give a convergent perturbation series despite the fact that the total e^+e^- cross section leads to a well-behaved perturbation series in this renormalization scheme. The problem of isolating and resumming the large terms is complicated by the fact that we do not have an analytic answer for the whole cross section. Moreover, in the piece for which we do have an analytic expression [eq. (3.26)], several large terms contribute to the overall large effect. Not all the terms have the same sign, so that by resumming one piece we may destroy a cancellation and aggravate the situation rather than improve it. In view of these difficulties, we limit ourselves to certain tentative suggestions.

In eq. (2.24) we noted the appearance of π^2 terms related to the soft singularity. Since the soft logarithms exponentiate it is presumably true that the π^2 terms also exponentiate. Under this assumption eq. (4.5) becomes

$$\frac{1}{\sigma}\int_{1/2}^{1}\frac{\mathrm{d}\sigma}{\mathrm{d}C}\,\mathrm{d}C \sim \exp\left(\frac{\alpha_s(Q^2)}{2\pi}\left(C_F+\tfrac{1}{2}N_C\right)\pi^2\right)2.8\left(\frac{\alpha_s(Q^2)}{2\pi}\right)\left(1+9\frac{\alpha_s(Q^2)}{2\pi}\right). \tag{4.6}$$

After extraction of the exponential, the remaining correction at PETRA energies would be in the perturbative range. To illustrate this point we have plotted in fig. 12 the total $O(\alpha_s^2)$ correction to $(C/\sigma)\,\mathrm{d}\sigma/\mathrm{d}C$, together with the $O(\alpha_s)$ contribution (fig. 3) multiplied by a factor $(\alpha_s/2\pi)(C_F+\frac{1}{2}N_C)\pi^2$. Independent of any exponentiation hypotheses, fig. 13 shows that the shape of the distribution is not substantially altered for values of $0.3 < C < 0.75$.

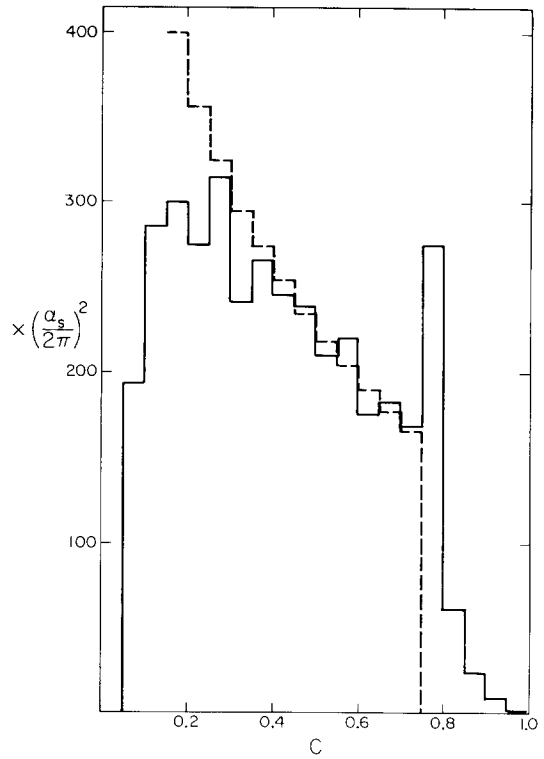

Fig. 12. The total $(C/\sigma)\,\mathrm{d}\sigma/\mathrm{d}C$ versus C (solid line). The lower-order $(C/\sigma)\,\mathrm{d}\sigma/\mathrm{d}C$ (fig. 3) multiplied by $(\alpha_s/2\pi)(2C_F + N_C)\pi^2$ versus C (dashed line). Both are plotted in units of $(\alpha_s/2\pi)^2$.

Eq. (3.26) also contains terms of the form

$$\frac{\alpha_s}{2\pi}\left(\tfrac{2}{3}T_R - \tfrac{11}{6}N_C\right)\ln(y_{13}y_{23}), \tag{4.7}$$

whose physical origin is that the four-momentum squared which determines the strength of the quark gluon coupling is not Q^2 but a smaller number. The running coupling constant should therefore be evaluated not at Q^2 but at Q^2 multiplied by a possibly C-dependent factor chosen to cancel as closely as possible the effect of the terms in eq. (4.7).

It appears that a reliable perturbative estimate for the fraction of multijet events will require a detailed understanding of the infrared singularities and the mass singularities, leading and subleading logs together with associated terms.

In fig. 13 we have plotted the total $\mathrm{d}\sigma/\mathrm{d}D$ versus D and its breakup into the group weight factors C_F^2, $C_F N_C$, $C_F T_R$. The bulk of the cross section is contained in the "QED-like" piece proportional to C_F^2. (The same is true for $(C/\sigma)\,\mathrm{d}\sigma/\mathrm{d}C$ in the purely four-jet region $C > \frac{3}{4}$, whereas for $C < \frac{3}{4}$ the C_F^2 and $C_F N_C$ pieces are of

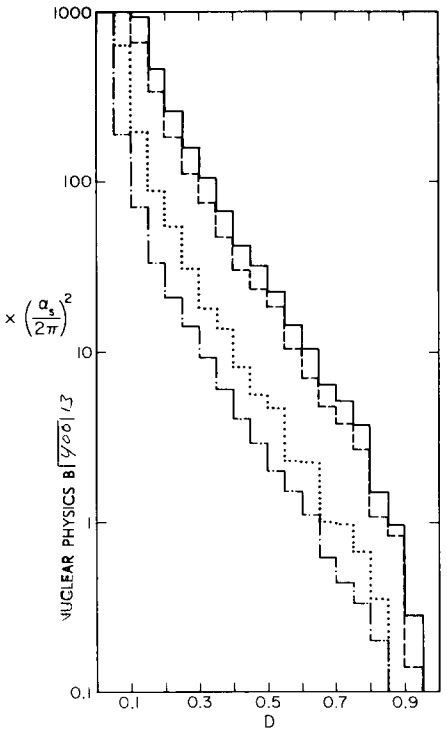

Fig. 13. $(1/\sigma)\mathrm{d}\sigma/\mathrm{d}D$ in units of $(\alpha_s/2\pi)^2$ plotted against D. The total is shown (solid line) together with C_F^2 part (dashed), $C_F N_C$ (dotted), $C_F T_R$ (dash-dotted).

similar size.) Whilst we cannot compare directly because we calculate different quantities, our results are in qualitative agreement with ref. [10].

Finally we have calculated the average values of C and D:

$$\langle C \rangle = \left(\frac{\alpha_s}{2\pi}\right) C_F (4\pi^2 - 33)\left(1 + 17\frac{\alpha_s}{2\pi}\right), \tag{4.8}$$

$$\langle D \rangle = \left(\frac{\alpha_s}{2\pi}\right)^2 60.5\,. \tag{4.9}$$

These average values are very sensitive to the effects of hadronization.

5. Conclusions

We have calculated the α_s^2 corrections to event shapes in e^+e^- annihilation using the perturbation theory of massless quarks and gluons and neglecting the fragmentation of these partons into final state hadrons. The results have been presented in terms of differential cross sections with respect to C and D. The

double differential cross section in C and D completely specifies the distribution in the eigenvalue plot (fig. 1), and hence the shape of the event. In order to obtain results which were free from infrared divergences it was necessary to calculate both the one-loop correction to the cross section for a three-parton final state and the tree diagram cross section for the production of four partons.

After integration of the four-jet cross section, both of the above contributions contain double and single poles. The potentially singular parts of the four-parton cross section are easily recognizable since they are proportional to a lower-order three-jet cross section folded with the appropriate Altarelli-Parisi kernel. However, in addition to these pieces the four-jet cross section contains singular terms not proportional to Altarelli-Parisi kernels which after integration contribute at the level of subleading logs. This confirms that the leading pole approximation can be used to obtain the coefficient of the leading but not the subleading logs. This, of course, does not alter the status of the KLN theorem; the infrared divergences of the two parts still cancel.

The histogram obtained for the differential cross section $(C/\sigma)\,\mathrm{d}\sigma/\mathrm{d}C$ displays such a large correction over the $O(\alpha_s)$ distribution that doubt is cast on the validity of the perturbation expansion. However, over a large range of C, $0.3 \lesssim C \lesssim 0.75$, this large correction is dominated by a π^2 which arises from a mismatch in the above-mentioned cancellation of double poles; the one-loop diagrams generate a $\ln^2(-Q^2)$ and the four-particle cross section has a $\ln^2(Q^2)$ with opposite sign. There is reason to believe that these π^2 terms can be summed to all orders giving a large exponential factor multiplying a convergent perturbation series. As we have emphasized in sect. 4, this procedure of selecting one of the large terms and resumming it is scarcely justifiable.

Notwithstanding this convergence problem, we find a large $O(\alpha_s^2)$ contribution to the differential cross section away from the two-jet region $C = 0$. The $O(\alpha_s^2)$ correction to the total cross section on the other hand is small eq. (2.16), so that the large corrections for $C \neq 0$ must be balanced by a large correction of opposite sign at $C = 0$.

Before these results may be compared with experimental data, the effects of hadronization should be taken into account. Hadronization is the process by which quarks and gluons arrange themselves into color singlet states by exchanging soft quarks and gluons. Logical consistency requires that the program of hadronization implemented when parton bremsstrahlung is taken into account should differ from that applied to the bare quark-antiquark jets, otherwise we run the risk of double counting. The converse of this statement is that the final-state interactions which we calculate represent the first primitive (non-confining) steps in the hadronization. Since the effects of hadronization fall like a power of the energy and the effects we calculate vanish only logarithmically there must exist an energy for which the perturbation series in $\alpha_s(Q^2)$ is a faithful approximation to QCD. At present energies we know that the hadronization will introduce significant smearing effects.

In particular the large negative correction at $C = 0$, when smeared out will reduce the calculated corrections for $C > 0$. This smearing of perturbative two-jet events should change only low values of C and the effects of hadronization at large values of C should be much less spectacular. If this hope is vindicated, and if the large contributions to the perturbation series can indeed be summed, we would expect a much larger multijet fraction, defined by making a lower cutoff on C, than previously estimated.

We are pleased to acknowledge useful discussions with R. P. Feynman, R. D. Field, T. Goldman, Z. Kunszt, H. D. Politzer, and S. Wolfram. We thank the MATHLAB at MIT for the use of MACSYMA.

Appendix A

In this appendix we give the values of the harder integrals used in the calculation. The first integral is required to isolate the singular piece of the four-jet cross section which contains a double pole:

$$I(x,y) = \int_0^x \mathrm{d}s\, s^{-1-\epsilon} \int_0^1 \mathrm{d}v \frac{v^{-\epsilon}(1-v)^{-\epsilon}}{(s+(y-s)v)},$$

$$I(x,y) = \frac{\Gamma^2(1-\epsilon)}{\Gamma(1-2\epsilon)} \frac{1}{y}\left[\frac{1}{2\epsilon^2} - \frac{\ln y}{2\epsilon} - \frac{1}{2}\ln^2\frac{x}{y} + \frac{1}{4}\ln^2 y - \mathrm{Li}_2\left(1-\frac{x}{y}\right) + \mathrm{O}(\epsilon)\right]. \tag{A.1}$$

The remaining two integrals are required for the calculation of the one-loop corrections to the three-jet cross section. Setting $Q^2 = (p_1+p_2+p_3)^2$ we have [21]

$$\int \frac{\mathrm{d}^n k}{(2\pi)^n} \frac{1}{k^2(k-p_2)^2(k+p_3)^2(k+p_1+p_3)^2}$$

$$= \frac{i}{16\pi^2}\left(-\frac{4\pi}{Q^2}\right)^{\epsilon} \frac{\Gamma(1+\epsilon)\Gamma^2(1-\epsilon)}{\Gamma(1-2\epsilon)} \frac{2}{s_{13}s_{23}}$$

$$\times\left[\frac{1}{\epsilon^2} - \frac{1}{\epsilon}\ln(y_{13}y_{23}) + \tfrac{1}{2}\ln^2 y_{13} + \tfrac{1}{2}\ln^2 y_{23} + R(y_{13},y_{23}) + \mathrm{O}(\epsilon)\right], \tag{A.2}$$

where $R(x,y)$ is given in eq. (2.22). Lastly, we have

$$\int \frac{d^n k}{(2\pi)^n} \frac{k\cdot p_1 k\cdot p_2}{(k+p_1)^2(k-p_2)^2(k+p_1+p_3)^2}$$

$$= \frac{i}{16\pi^2}\left(-\frac{4\pi}{Q^2}\right)^{\varepsilon} \frac{\Gamma(1+\varepsilon)\Gamma^2(1-\varepsilon)}{\Gamma(2-2\varepsilon)}$$

$$\times\left\{-\frac{1}{\varepsilon}\left[\frac{s_{12}^2 s_{13}^2 \ln y_{12}}{4(s_{13}+s_{23})^3} + \frac{s_{13}s_{23}^2 + s_{13}^2 s_{23} + s_{12}(s_{13}^2 - 2s_{13}s_{23} - s_{23}^2)}{8(s_{13}+s_{23})^2}\right]\right.$$

$$\left. + \frac{s_{12}s_{13}s_{23}}{4(s_{13}+s_{23})^2} + \frac{s_{12}^2 \ln y_{12}(s_{13}^2 \ln y_{12} + s_{23}^2 + s_{13}^2 + 4s_{13}s_{23})}{8(s_{13}+s_{23})^3} + O(\varepsilon)\right\}. \tag{A.3}$$

Appendix B

In this appendix we present the differential cross section calculated in order α_s^2 for the production of a four-parton final state. The reaction $e^+e^- \to q\bar{q}GG$ gives a contribution,

$$\frac{1}{\sigma_0} d\sigma^{(4)} = C_F\left(\frac{\alpha_s}{2\pi}\right)^2 \tfrac{1}{2} Q^2 \int dy_{123} \int dy_{134} \int dy_{13} \theta(y_{13})\theta(y_{123}y_{134} - y_{13})$$

$$\times \theta(y_{13} + 1 - y_{123} - y_{134}) \int_0^1 dv \frac{1}{\pi}\int_0^\pi d\theta'$$

$$\times \{(A+B+C) + (1\Leftrightarrow 2) + (3\Leftrightarrow 4) + (1\Leftrightarrow 2, 3\Leftrightarrow 4)\}. \tag{B.1}$$

The reaction $e^+e^- \to \bar{q}\bar{q}qq$ gives the contribution,

$$\frac{1}{\sigma_0} d\sigma^{(4)} = C_F\left(\frac{\alpha_s}{2\pi}\right)^2 \tfrac{1}{4} Q^2 \int dy_{123} \int dy_{134} \int dy_{13} \theta(y_{13})\theta(y_{123}y_{134} - y_{13})$$

$$\times \theta(y_{13} + 1 - y_{123} - y_{134}) \int_0^1 dv \frac{1}{\pi}\int_0^\pi d\theta'$$

$$\times \{(D+E) + (1\Leftrightarrow 2) + (3\Leftrightarrow 4) + (1\Leftrightarrow 2, 3\Leftrightarrow 4)\}, \tag{B.2}$$

where the quantities v and θ' are defined by eqs. (3.2–3.5). The quantities A, B, C, D and E are given in the following equations. Our results for the matrix element for

the first reaction are in agreement with the results of Ali et al., (ref. [10]) except for a typing error which will be corrected in the published version of their paper.

$$A = C_F\{(s_{12}s_{34}^2 - s_{13}s_{24}s_{34} + s_{14}s_{23}s_{34} + 3s_{12}s_{23}s_{34} + 3s_{12}s_{14}s_{34} + 4s_{12}^2s_{34} - s_{13}s_{23}s_{24}$$
$$+ 2s_{12}s_{23}s_{24} - s_{13}s_{14}s_{24} - 2s_{12}s_{13}s_{24} + 2s_{12}^2s_{24} + s_{14}s_{23}^2 + 2s_{12}s_{23}^2 + s_{14}^2s_{23}$$
$$+ 4s_{12}s_{14}s_{23} + 4s_{12}^2s_{23} + 2s_{12}s_{14}^2 + 2s_{12}s_{13}s_{14} + 4s_{12}^2s_{14} + 2s_{12}^2s_{13} + 2s_{12}^3)$$
$$/(2s_{13}s_{134}s_{234}s_{24}) + (s_{24}s_{34} + s_{12}s_{34} + s_{13}s_{24} - s_{14}s_{23} + s_{12}s_{13})$$
$$/(s_{13}s_{134}^2) + 2s_{23}(Q^2 - s_{13})/(s_{13}s_{134}s_{24}) + s_{34}/(2s_{13}s_{24})\}, \qquad \text{(B.3)}$$

$$B = (C_F - \tfrac{1}{2}N_C)\{(s_{12}s_{24}s_{34} + s_{12}s_{14}s_{34} - s_{13}s_{24}^2 + s_{13}s_{14}s_{24} + 2s_{12}s_{14}s_{24})$$
$$/(s_{13}s_{134}s_{23}s_{14}) + s_{12}(Q^2 + s_{34})s_{124}/(s_{134}s_{234}s_{14}s_{24}) - (2s_{13}s_{24} + s_{14}^2$$
$$+ s_{13}s_{23} + 2s_{12}s_{13})/(s_{13}s_{134}s_{14}) + s_{12}s_{123}s_{124}/(2s_{13}s_{14}s_{23}s_{24})\}, \qquad \text{(B.4)}$$

$$C = N_C\{-(5s_{12}s_{34}^2 + 2s_{12}s_{24}s_{34} + 2s_{12}s_{23}s_{34} + 2s_{12}s_{14}s_{34} + 2s_{12}s_{13}s_{34}$$
$$+ 4s_{12}^2s_{34} - s_{13}s_{24}^2 + s_{14}s_{23}s_{24} + s_{13}s_{23}s_{24} + s_{13}s_{14}s_{24} - s_{12}s_{14}s_{24} - s_{13}^2s_{24}$$
$$- 3s_{12}s_{13}s_{24} - s_{14}s_{23}^2 - s_{14}^2s_{23} + s_{13}s_{14}s_{23}$$
$$- 3s_{12}s_{14}s_{23} - s_{12}s_{13}s_{23})/(4s_{134}s_{234}s_{34}^2)$$

$$+ (3s_{12}s_{34}^2 - 3s_{13}s_{24}s_{34} + 3s_{12}s_{24}s_{34} + 3s_{14}s_{23}s_{34} - s_{13}s_{24}^2$$
$$- s_{12}s_{23}s_{34} + 6s_{12}s_{14}s_{34} + 2s_{12}s_{13}s_{34} - 2s_{12}^2s_{34} + s_{14}s_{23}s_{24} - 3s_{13}s_{23}s_{24}$$
$$- 2s_{13}s_{14}s_{24} + 4s_{12}s_{14}s_{24} + 2s_{12}s_{13}s_{24} + 3s_{14}s_{23}^2 + 2s_{14}^2s_{23} + 2s_{14}^2s_{12}$$
$$+ 2s_{12}^2s_{14} + 6s_{12}s_{14}s_{23} - 2s_{12}s_{13}^2 - 2s_{12}^2s_{13})/(4s_{13}s_{134}s_{234}s_{34})$$

$$+ (2s_{12}s_{34}^2 - 2s_{13}s_{24}s_{34} + s_{12}s_{24}s_{34} + 4s_{13}s_{23}s_{34} + 4s_{12}s_{14}s_{34}$$
$$+ 2s_{12}s_{13}s_{34} + 2s_{12}^2s_{34} - s_{13}s_{24}^2 + 3s_{14}s_{23}s_{24} + 4s_{13}s_{23}s_{24} - 2s_{13}s_{14}s_{24}$$
$$+ 4s_{12}s_{14}s_{24} + 2s_{12}s_{13}s_{24} + 2s_{14}s_{23}^2 + 4s_{13}s_{23}^2 + 2s_{13}s_{14}s_{23} + 2s_{12}s_{14}s_{23}$$
$$+ 4s_{12}s_{13}s_{23} + 2s_{12}s_{14}^2 + 4s_{12}^2s_{13} + 4s_{12}s_{13}s_{14} + 2s_{12}^2s_{14})/(4s_{13}s_{134}s_{24}s_{34})$$

$$
\begin{aligned}
&- \big(s_{12}s_{34}^2 - 2s_{14}s_{24}s_{34} - 2s_{13}s_{24}s_{34} \\
&\quad - s_{14}s_{23}s_{34} + s_{13}s_{23}s_{34} + s_{12}s_{14}s_{34} + 2s_{12}s_{13}s_{34} - 2s_{14}^2 s_{24} - 4s_{13}s_{14}s_{24} \\
&\quad - 4s_{13}^2 s_{24} - s_{14}^2 s_{23} - s_{13}^2 s_{23} + s_{12}s_{13}s_{14} - s_{12}s_{13}^2\big)/\big(2s_{13}s_{34}s_{134}^2\big) \\
&+ \big(s_{12}s_{34}^2 - 4s_{14}s_{24}s_{34} - 2s_{13}s_{24}s_{34} - 2s_{14}s_{23}s_{34} - 4s_{13}s_{23}s_{34} - 4s_{12}s_{14}s_{34} \\
&\quad - 4s_{12}s_{13}s_{34} - 2s_{13}s_{14}s_{24} + 2s_{13}^2 s_{24} + 2s_{14}^2 s_{23} - 2s_{13}s_{14}s_{23} - s_{12}s_{14}^2 \\
&\quad - 6s_{12}s_{13}s_{14} - s_{12}s_{13}^2\big)/\big(4s_{34}^2 s_{134}^2\big)\big\}\,, \qquad \text{(B.5)}
\end{aligned}
$$

$$
\begin{aligned}
D = T_R\big\{\big[&\big(s_{13}s_{23}s_{34} + s_{12}s_{23}s_{34} - s_{12}^2 s_{34} + s_{13}s_{23}s_{24} + 2s_{12}s_{23}s_{24} - s_{14}s_{23}^2 \\
&+ s_{12}s_{13}s_{24} + s_{12}s_{14}s_{23} + s_{12}s_{13}s_{14}\big)/\big(s_{13}^2 s_{123}^2\big) - \big(s_{12}s_{34}^2 - s_{13}s_{24}s_{34} \\
&+ s_{12}s_{24}s_{34} - s_{14}s_{23}s_{34} - s_{12}s_{23}s_{34} - s_{13}s_{24}^2 + s_{14}s_{23}s_{24} - s_{13}s_{23}s_{24} \\
&- s_{13}^2 s_{24} + s_{14}s_{23}^2\big)/\big(s_{13}^2 s_{123}s_{134}\big)\big] + \big[(1\Leftrightarrow 3, 2\Leftrightarrow 4)\big]\big\}\,, \qquad \text{(B.6)}
\end{aligned}
$$

$$
\begin{aligned}
E = \big(C_F - \tfrac{1}{2}N_C\big)\big\{\big[&\big(s_{12}s_{23}s_{34} - s_{12}s_{24}s_{34} + s_{12}s_{14}s_{34} + s_{12}s_{13}s_{34} + s_{13}s_{24}^2 \\
&- s_{14}s_{23}s_{24} + s_{13}s_{23}s_{24} + s_{13}s_{14}s_{24} + s_{13}^2 s_{24} - s_{14}s_{23}^2 - s_{14}^2 s_{23} - s_{13}s_{14}s_{23}\big) \\
&/\big(s_{13}s_{23}s_{123}s_{134}\big) - s_{12}\big(s_{12}s_{34} - s_{23}s_{24} - s_{13}s_{24} - s_{14}s_{23} - s_{14}s_{13}\big) \\
&/\big(s_{13}s_{23}s_{123}^2\big) - \big(s_{14} + s_{13}\big)\big(s_{24} + s_{23}\big)s_{34}/\big(s_{13}s_{23}s_{134}s_{234}\big)\big] \\
&+ \big[(1\Leftrightarrow 3, 2\Leftrightarrow 4)\big]\big\}\,. \qquad \text{(B.7)}
\end{aligned}
$$

References

[1] S. Orito et al., JADE Collaboration, Proc. Int. Symp. on Lepton and photon interactions at high energies (FNAL, Batavia, 1979);
D.P. Barber et al., Mark-J Collaboration, Phys. Rev. Lett. 43 (1979) 830;
Ch. Berger et al., PLUTO Collaboration, Phys. Lett. 86B (1979) 418;
R. Brandelik et al., TASSO Collaboration, Phys. Lett. 86B (1979) 243

[2] J. Ellis, M.K. Gaillard and G.G. Ross, Nucl. Phys. B111 (1976) 253; (E:B130 (1977) 516)

[3] C.L. Basham, L.S. Brown, S.D. Ellis and S.T. Love, Phys. Rev. D17 (1978) 2298; Phys. Rev. Lett. 41 (1978) 1585;
H. Georgi and M. Machacek, Phys. Rev. Lett. 39 (1977) 1237;
E. Farhi, Phys. Rev. Lett. 39 (1977) 1587;
A. De Rújula, J. Ellis, E.G. Floratos and M.K. Gaillard, Nucl. Phys. B138 (1978) 387;

S.Y. Pi, R.L. Jaffe and F.E. Low, Phys. Rev. Lett. 41 (1978) 142;
S.S. Shei, Phys. Lett. 79B (1978) 245;
K. Shizuya and S.-H.H. Tye, Phys. Rev. Lett. 41 (1978) 1195;
T.A. DeGrand, Y.J. Ng and S.-H.H. Tye, Phys. Rev. D16 (1977) 3251
[4] G.C. Fox and S. Wolfram, Phys. Rev. Lett. 41 (1978) 1581; Nucl Phys. B149 (1979) 413; Phys. Lett. 82B (1979) 134
[5] G. Sterman and S. Weinberg, Phys. Rev. Lett. 39 (1977) 1436
[6] G. Parisi, Phys. Lett. 74B (1978) 65
[7] J.F. Donoghue, F.E. Low and S.Y. Pi, Phys. Rev. D20 (1979) 2759
[8] S.L. Wu and G. Zobernig, Z. Phys. C2 (1979) 107
[9] T. Kinoshita, J. Math. Phys. 3 (1962) 650;
T.D. Lee and M. Nauenberg, Phys. Rev. 133 (1964) 1549
[10] A. Ali, J.G. Körner, Z. Kunszt, J. Willrodt, G. Schierholz and E. Pietarinen, Phys. Lett. 82B (1979) 285; DESY report 79/54 (1979); Nucl. Phys. B, to be published;
K.J.F. Gaemers and J.A.M. Vermaseren, CERN preprint TH 2816
[11] G. 't Hooft and M. Veltman, Nucl. Phys. B44 (1972) 189;
C.G. Bollini and J.J. Giambiagi, Nuovo Cim. 12B (1972) 20;
W.J. Marciano, Phys. Rev. D12 (1975) 3861
[12] A.E. Terrano and S. Wolfram, Caltech report in preparation;
S. Wolfram, MACSYMA tools for Feynman diagram calculation, Proc. 1979 MACSYMA Users' Conf., ed. V.E. Lewis, Washington, 1979; Caltech preprint CALT-68-736.
[13] MATHLAB Group, MIT Laboratory for Computer Science, MACSYMA Primer, (March, 1978) and MACSYMA Reference Manual, Version 9 (Dec., 1977)
[14] W.A. Bardeen, A.J. Buras, D.W. Duke and T. Muta, Phys. Rev. D18 (1978) 3998
[15] T. Appelquist and H. Georgi, Phys. Rev. D8 (1973) 4000;
A. Zee, Phys. Rev. D8 (1973) 4038
[16] M. Dine and J. Sapirstein, Phys. Rev. Lett. 43 (1979) 668;
W. Celmaster and R.J. Gonsalves, UCSD preprint-10P10-206, 207 (1979);
K.G. Chetyrkin, A.L. Kataev and F.V. Tkachov, Phys. Lett. 85B (1979) 277
[17] W. Caswell, Phys. Rev. Lett. 33 (1974) 244;
D.R.T. Jones, Nucl. Phys. B75 (1974) 531
[18] G. Altarelli and G. Parisi, Nucl. Phys. B126 (1977) 298;
G. Parisi, Proc. 11th Rencontre de Moriond, 1976, ed., J. Tran Thanh Van
[19] W. Furry, Phys. Rev. 51 (1937) 125
[20] P. Binétruy, Phys. Lett. 91B (1980) 245
[21] K. Fabricius and I. Schmitt, Z. Phys. C3 (1979) 51